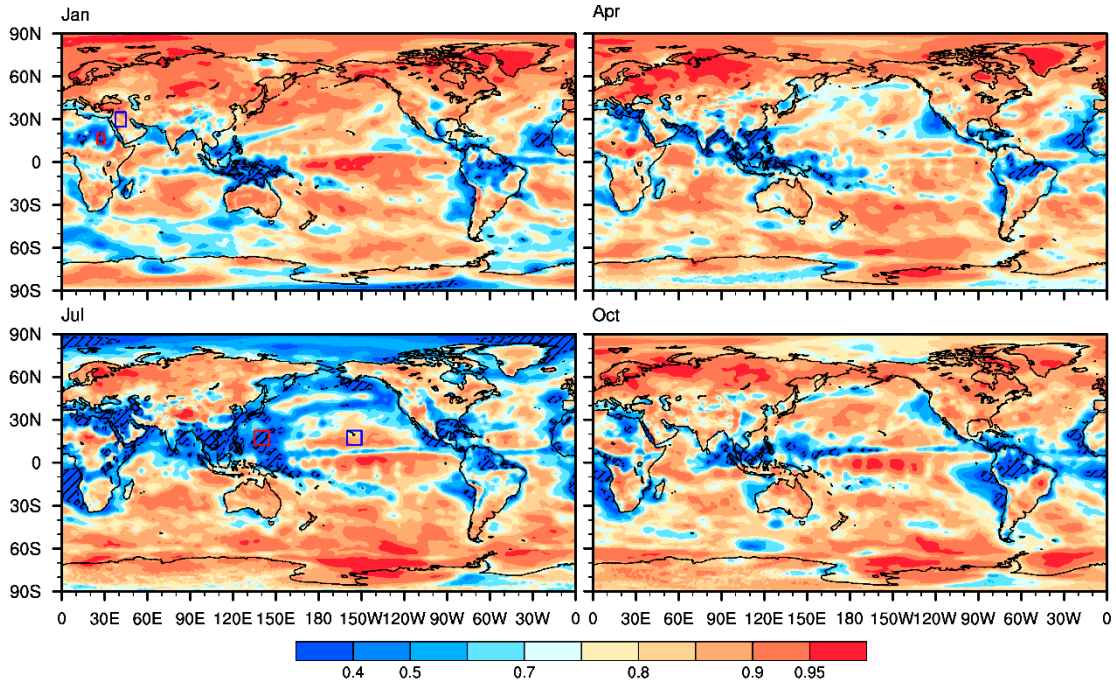# Supplementary Materials

Figure S1. Maps of correlation coefficients of PW and SVP (The dataset used is JRA55). The correlation coefficients in shaded areas cannot pass the 0.05 significance level. Blue and red squares are strong and weak correlation areas respectively selected to show the vertical profiles.

Figure S2. Maps of correlation coefficients of PW and SVP (The dataset used is NCEP2). The correlation coefficients in shaded areas cannot pass the 0.05 significance level. Blue and red squares

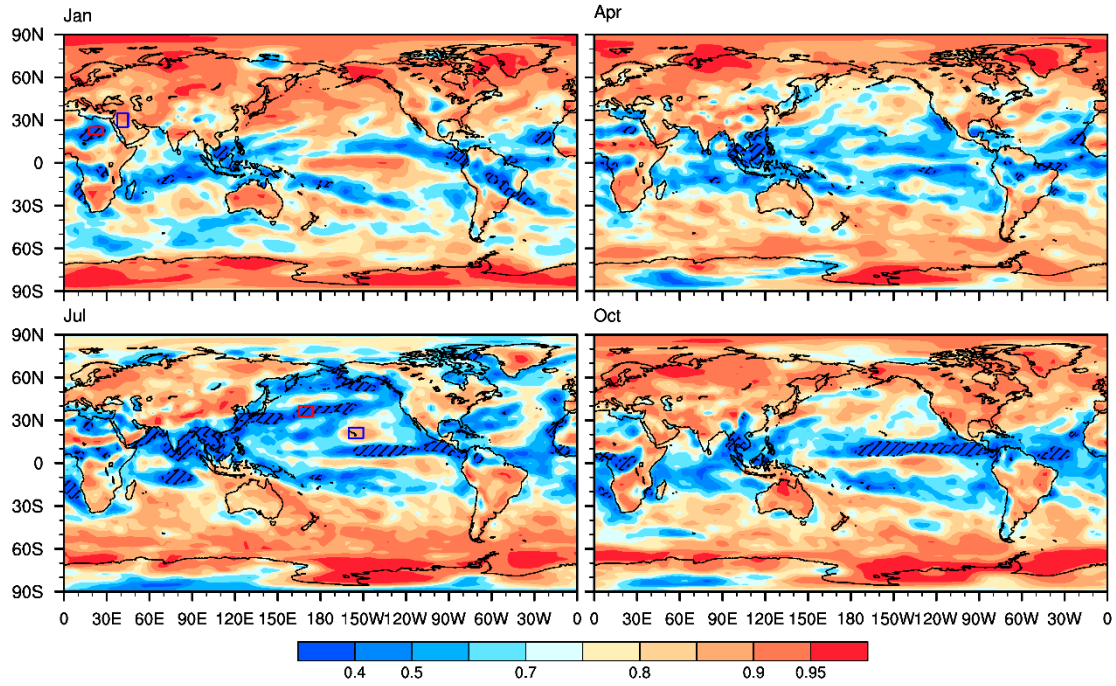are strong and weak correlation areas respectively selected to show the vertical profiles
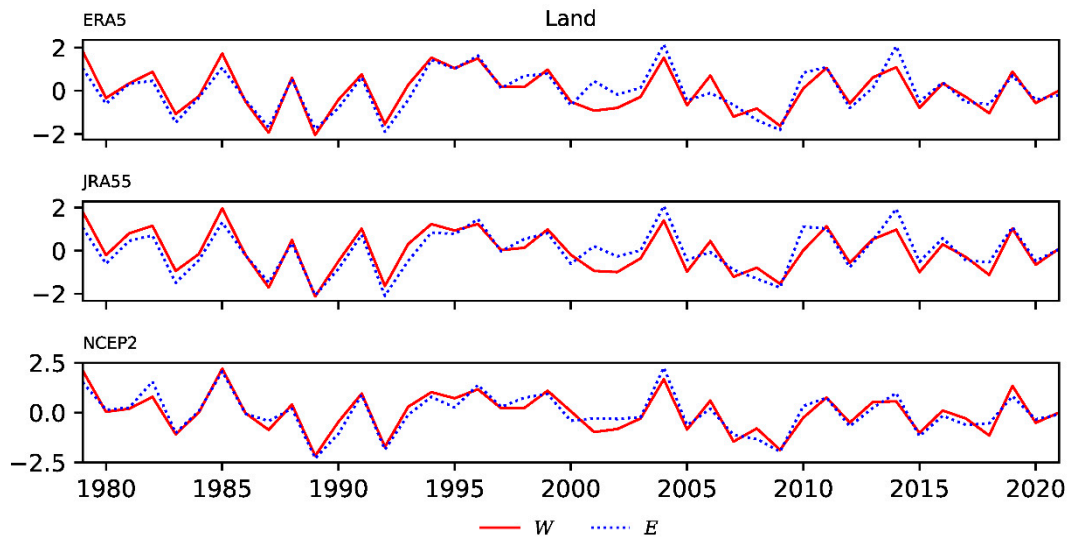

Figure S3. The curves of normalized PW and SVP in strong correlation areas on land (blue squares in January in Fig. 1, Fig. S1, and Fig. S2).
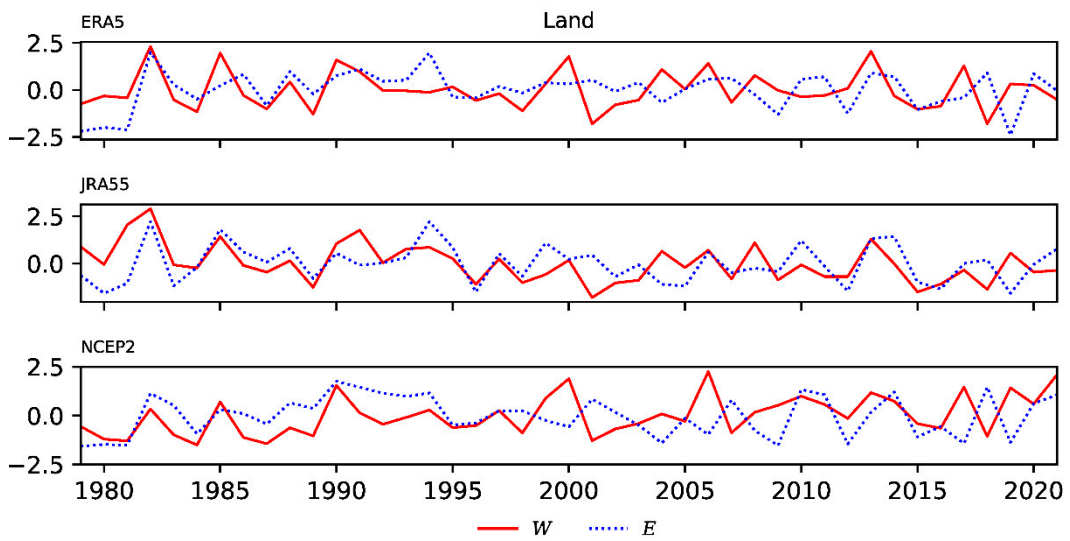

Figure S4. The curves of normalized PW and SVP in weak correlation areas on land (red squares in January in Fig. 1, Fig. S1, and Fig. S2).
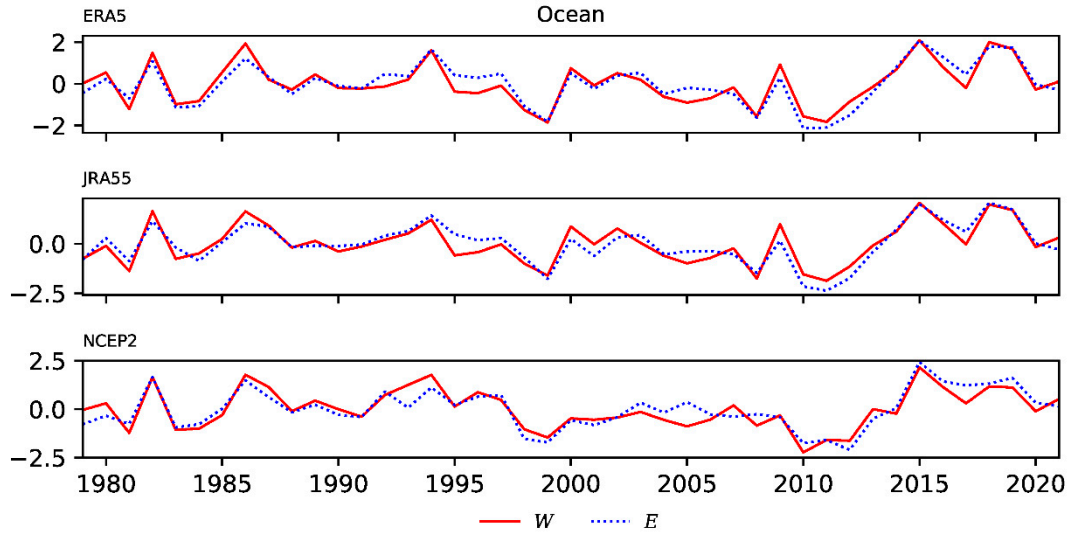
Figure S5. The curves of normalized PW and SVP in strong correlation areas over the oceans (blue squares in July in Fig. 1, Fig. S1, and Fig. S2).
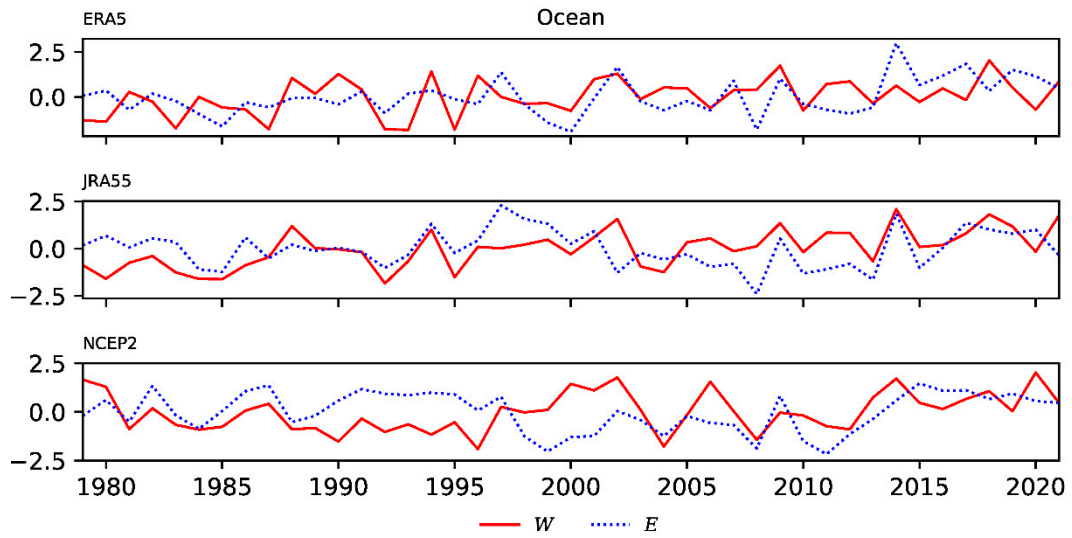

Figure S6. The curves of normalized PW and SVP in weak correlation areas (red squares in July in Fig. 1-3) over the oceans.
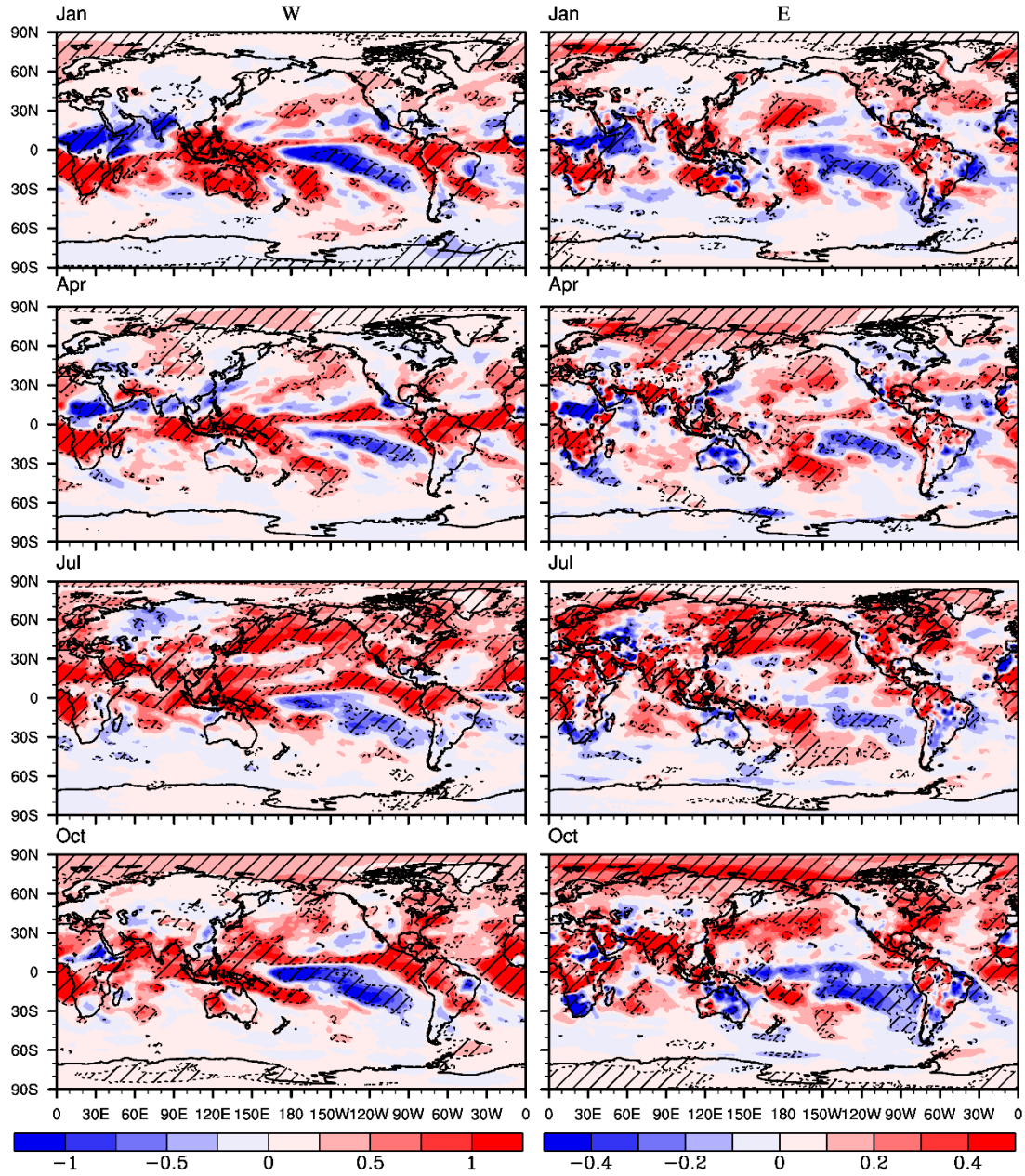
Figure S7. The long-term trends of PW (the left column, unit: kg·m⁻²/10yr) and SVP (the right column, unit: hPa/10yr) in four months calculated with the JRA55 dataset. The rows from top to bottom respond to January, April, July, and October respectively. Trends in the shaded areas can reach the 0.05 significance level.

Figure S8. The long-term trends of PW (the left column, unit: kg·m⁻²/10yr) and SVP (the right column, unit: hPa/10yr) in four months calculated with the NCEP2 dataset. The rows from top to bottom respond to January, April, July, and October respectively. Trends in the shaded areas can reach the 0.05 significance level.
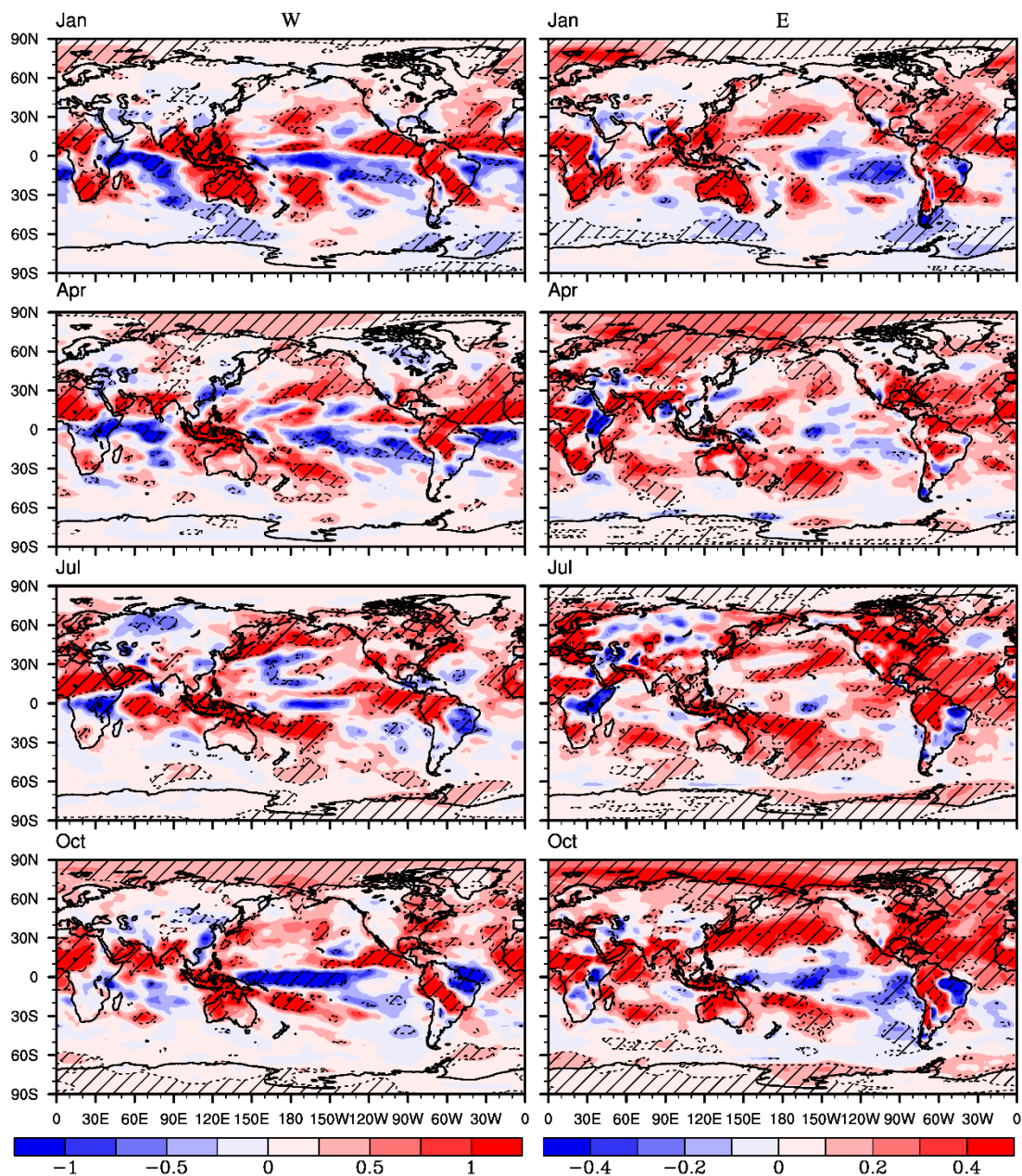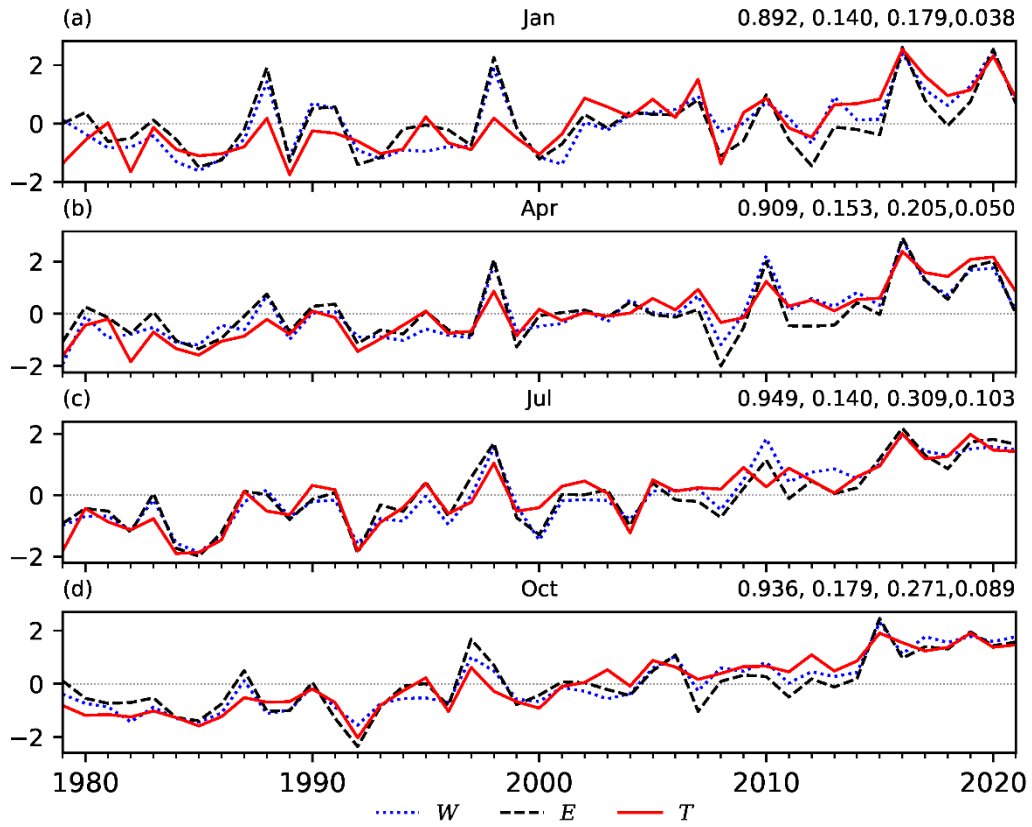
Figure S9. The time series of normalized global areal-weighted averages of 2 m temperature (T), PW (W), and SVP (E) in January (**a**), April (**b**), July (**c**), and October (**d**) calculated with JRA55 datasets. The four numbers at the top-right of subgraphs are the correlation coefficient between PW and SVP and Sen's slope value of three elements (T, W, and E in sequence; units: K/10yr, kg·m^{-2}/10 yr, and hPa/10yr), separately.
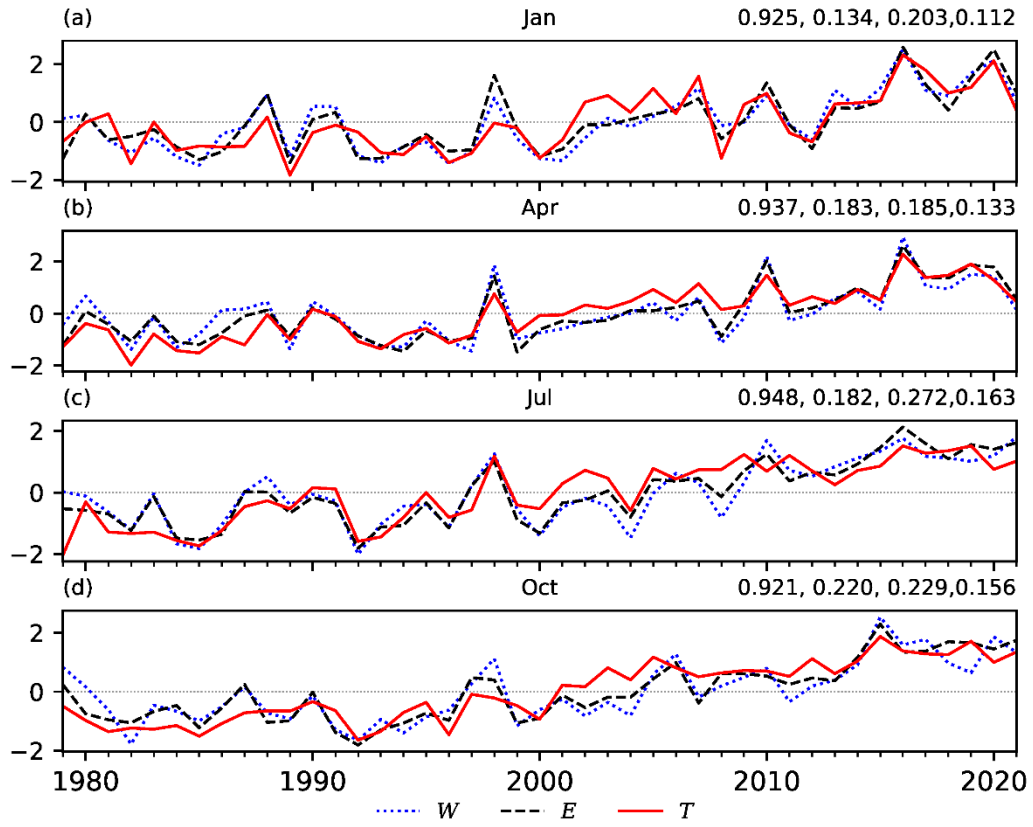
Figure S10. The time series of normalized global areal-weighted averages of 2 m temperature (*T*), PW (*W*), and SVP (*E*) in January (**a**), April (**b**), July (**c**), and October (**d**) calculated with NCEP2 datasets. The four numbers at the top-right of subgraphs are the correlation coefficient between PW and SVP and Sen's slope value of three elements (*T*, *W*, and *E* in sequence; units: K/10yr, kg·m^{-2}/10 yr, and hPa/10yr), separately.
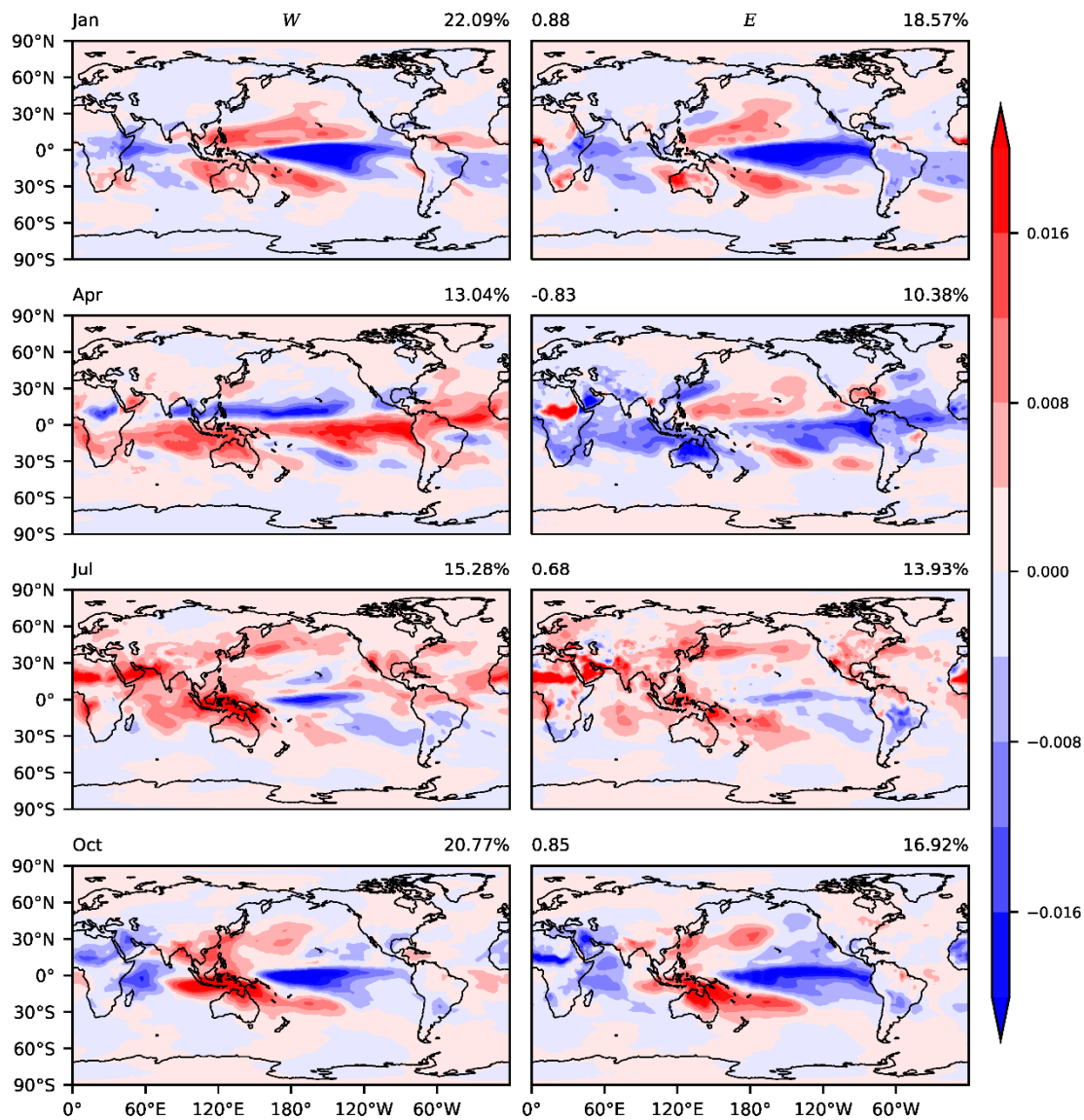
Figure S11. The first EOF modes of PW (left) and SVP (right) calculated with JRA55. (The rows from top to bottom correspond to January, April, July, and October respectively. The percentages at the top-right of subgraphs are fractional mode variances corresponding to PW and SVP. The numbers at the upper-left corners of graphs in the right column are spatial correlation coefficients of the first modes of PW and SVP.).

Figure S12. The first EOF modes of PW (left) and SVP (right) calculated with NCEP2. (The rows from top to bottom correspond to January, April, July, and October respectively. The percentages at the top-right of subgraphs are fractional mode variances corresponding to PW and SVP. The numbers at the upper-left corners of graphs in the right column are spatial correlation coefficients of the first modes of PW and SVP.).
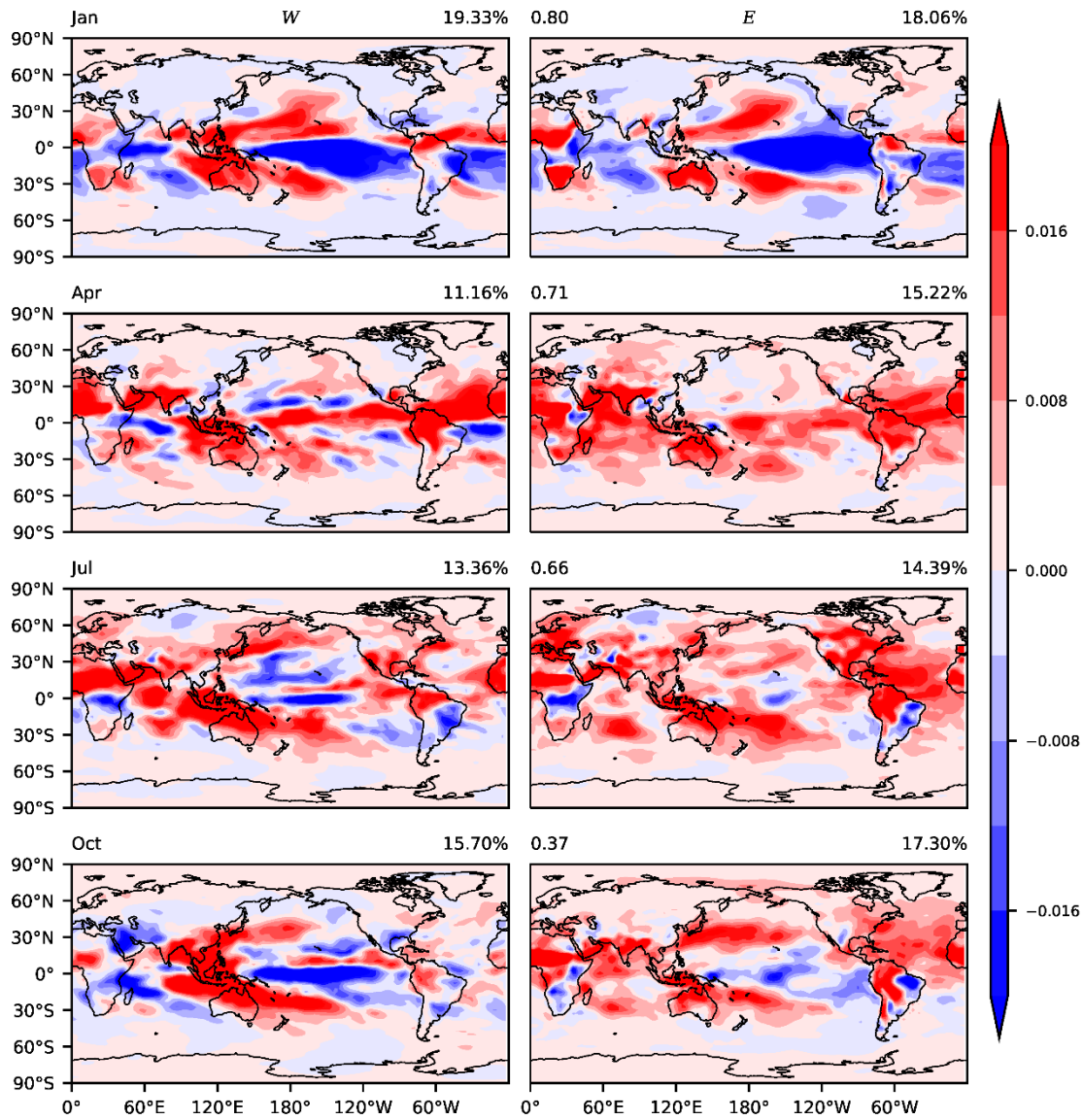
Figure S13. The second EOF modes of PW (left) and SVP (right) calculated with ERA5. (The rows from top to bottom correspond to January, April, July, and October respectively. The percentages at the top-right of subgraphs are fractional mode variances corresponding to PW and SVP. The numbers at the upper-left corners of graphs in the right column are spatial correlation coefficients of the first modes of PW and SVP.).
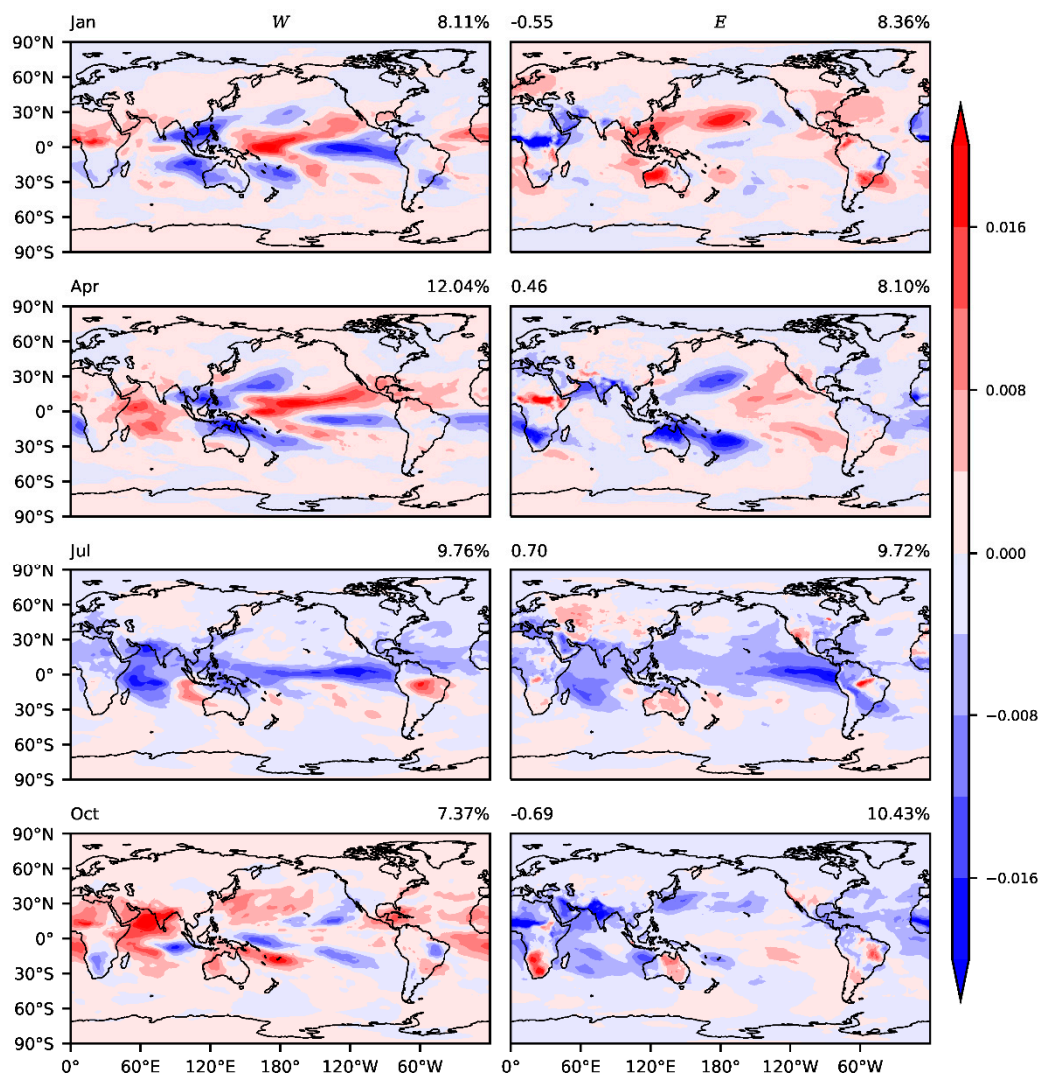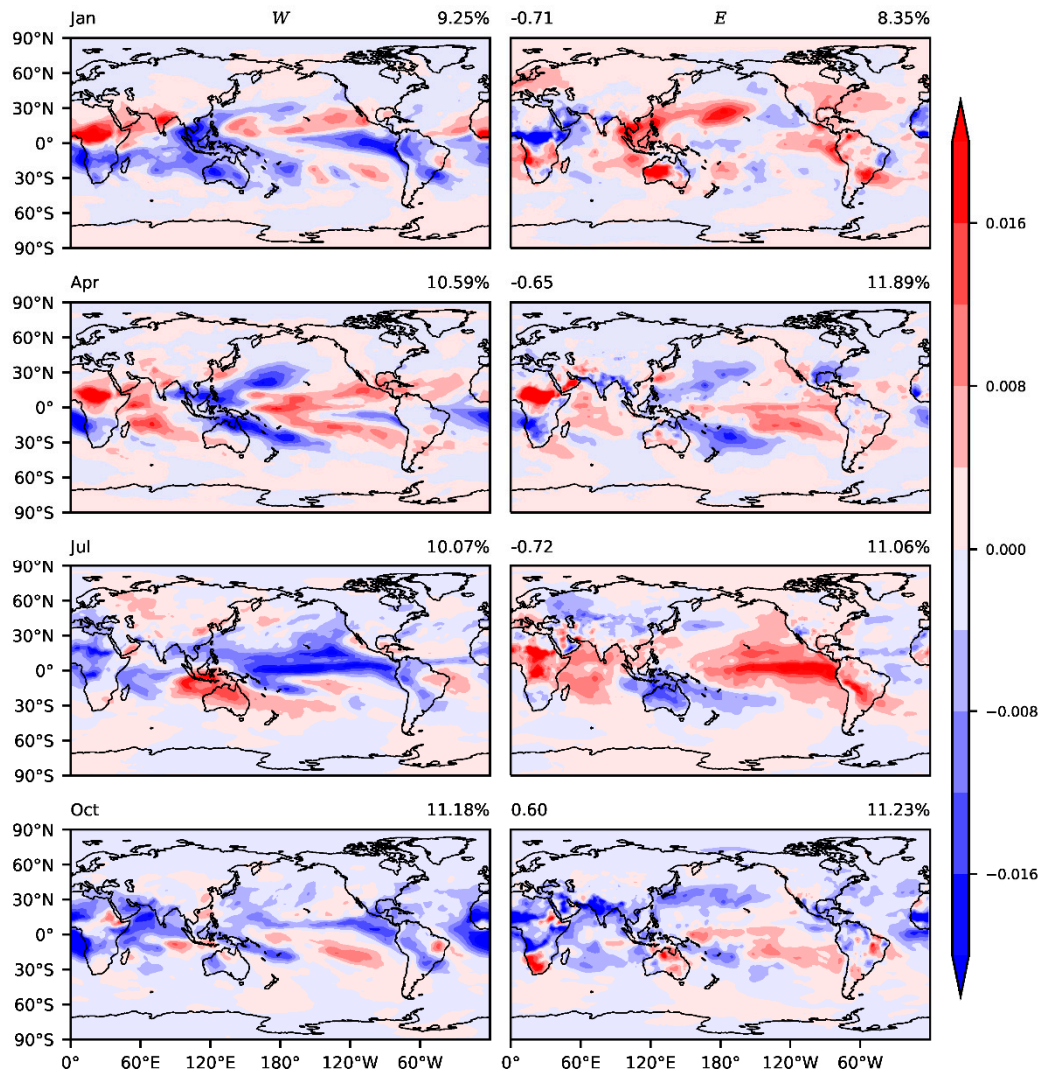
Figure S14. The second EOF modes of PW (left) and SVP (right) calculated with JRA55. (The rows from top to bottom correspond to January, April, July, and October respectively. The percentages at the top-right of subgraphs are fractional mode variances corresponding to PW and SVP. The numbers at the upper-left corners of graphs in the right column are spatial correlation coefficients of the first modes of PW and SVP.).
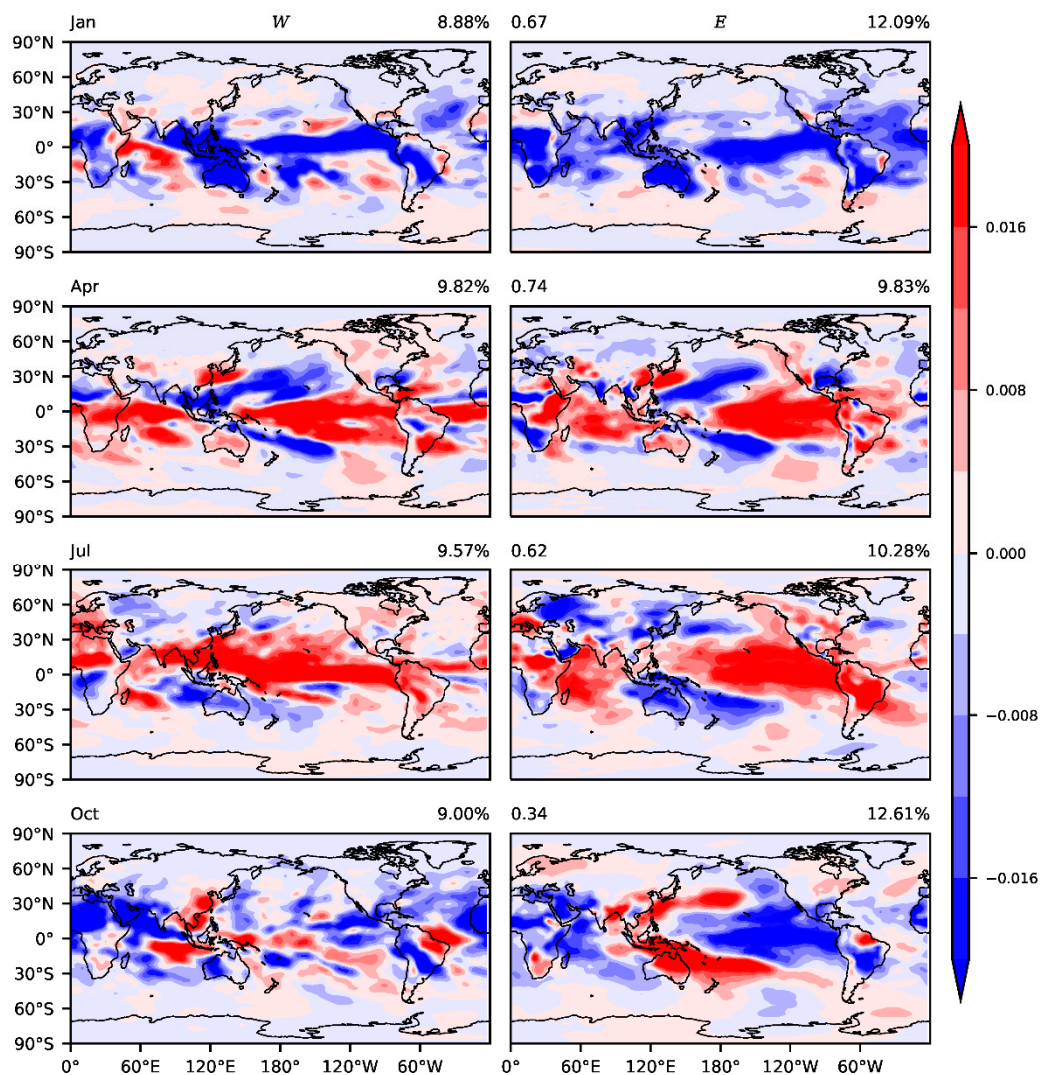
Figure S15. The second EOF modes of PW (left) and SVP (right) calculated with ncep2. (The rows from top to bottom correspond to January, April, July, and October respectively. The percentages at the top-right of subgraphs are fractional mode variances corresponding to PW and SVP. The numbers at the upper-left corners of graphs in the right column are spatial correlation coefficients of the first modes of PW and SVP.).
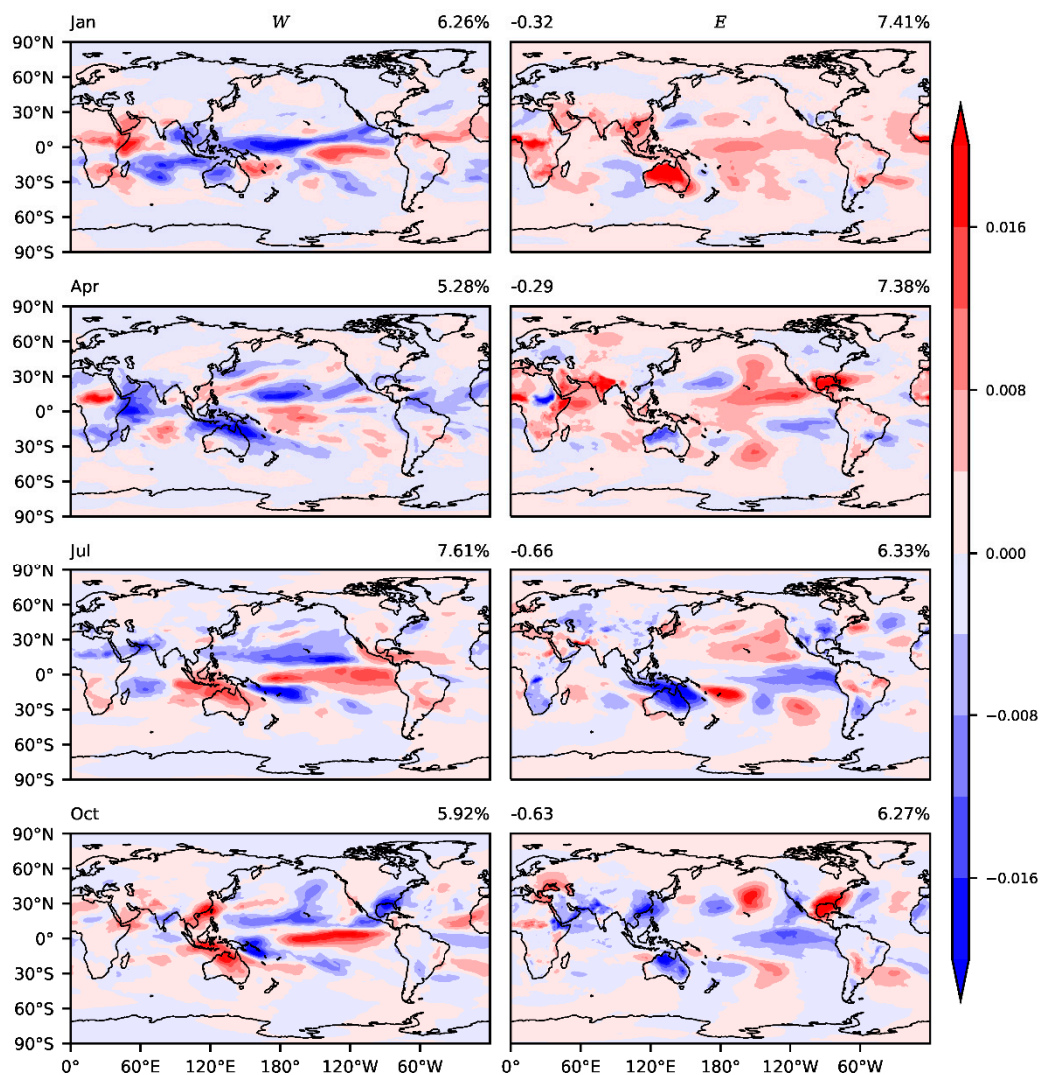
Figure S16. The third EOF modes of PW (left) and SVP (right) calculated with ERA5. (The rows from top to bottom correspond to January, April, July, and October respectively. The percentages at the top-right of subgraphs are fractional mode variances corresponding to PW and SVP. The numbers at the upper-left corners of graphs in the right column are spatial correlation coefficients of the first modes of PW and SVP.).
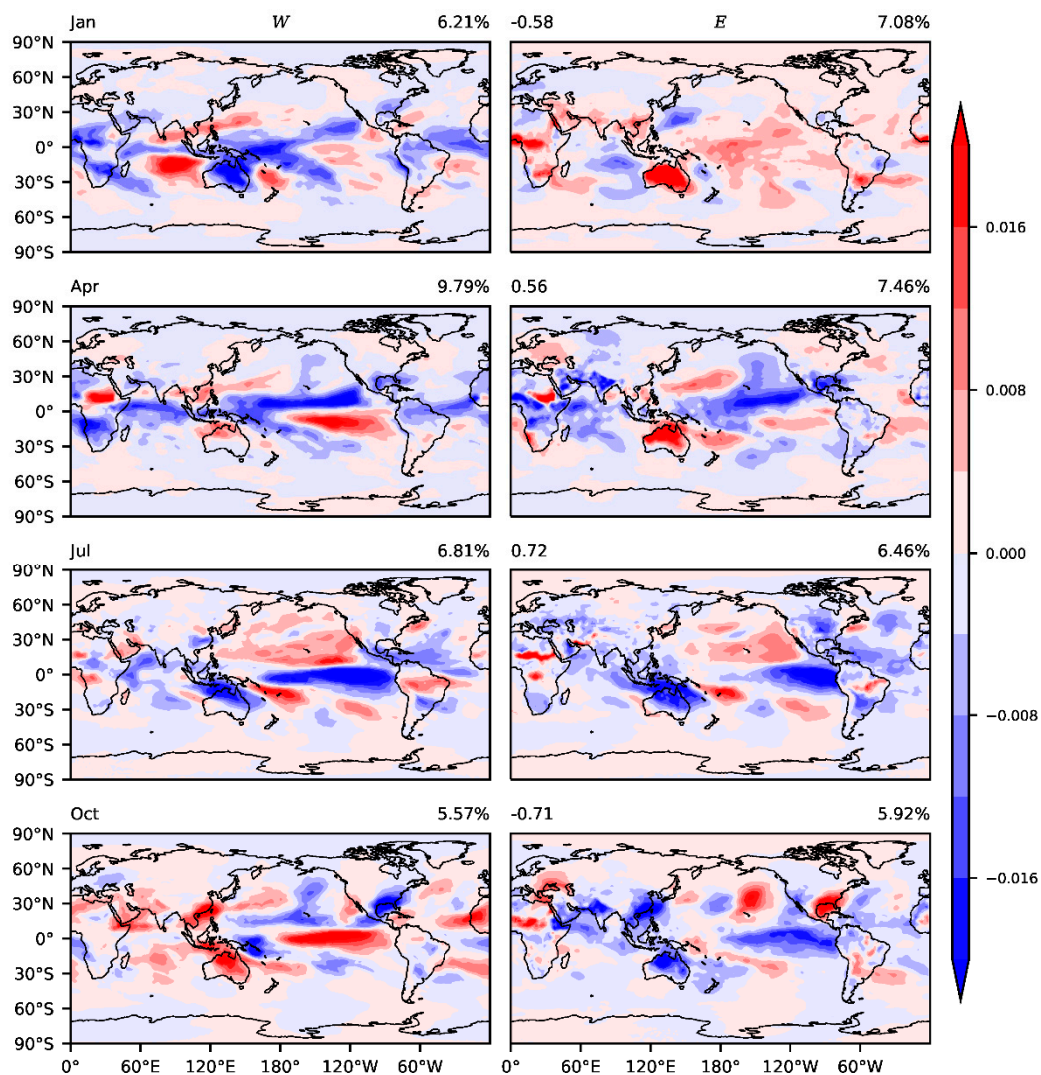
Figure S17. The third EOF modes of PW (left) and SVP (right) calculated with JRA55. (The rows from top to bottom correspond to January, April, July, and October respectively. The percentages at the top-right of subgraphs are fractional mode variances corresponding to PW and SVP. The numbers at the upper-left corners of graphs in the right column are spatial correlation coefficients of the first modes of PW and SVP.).
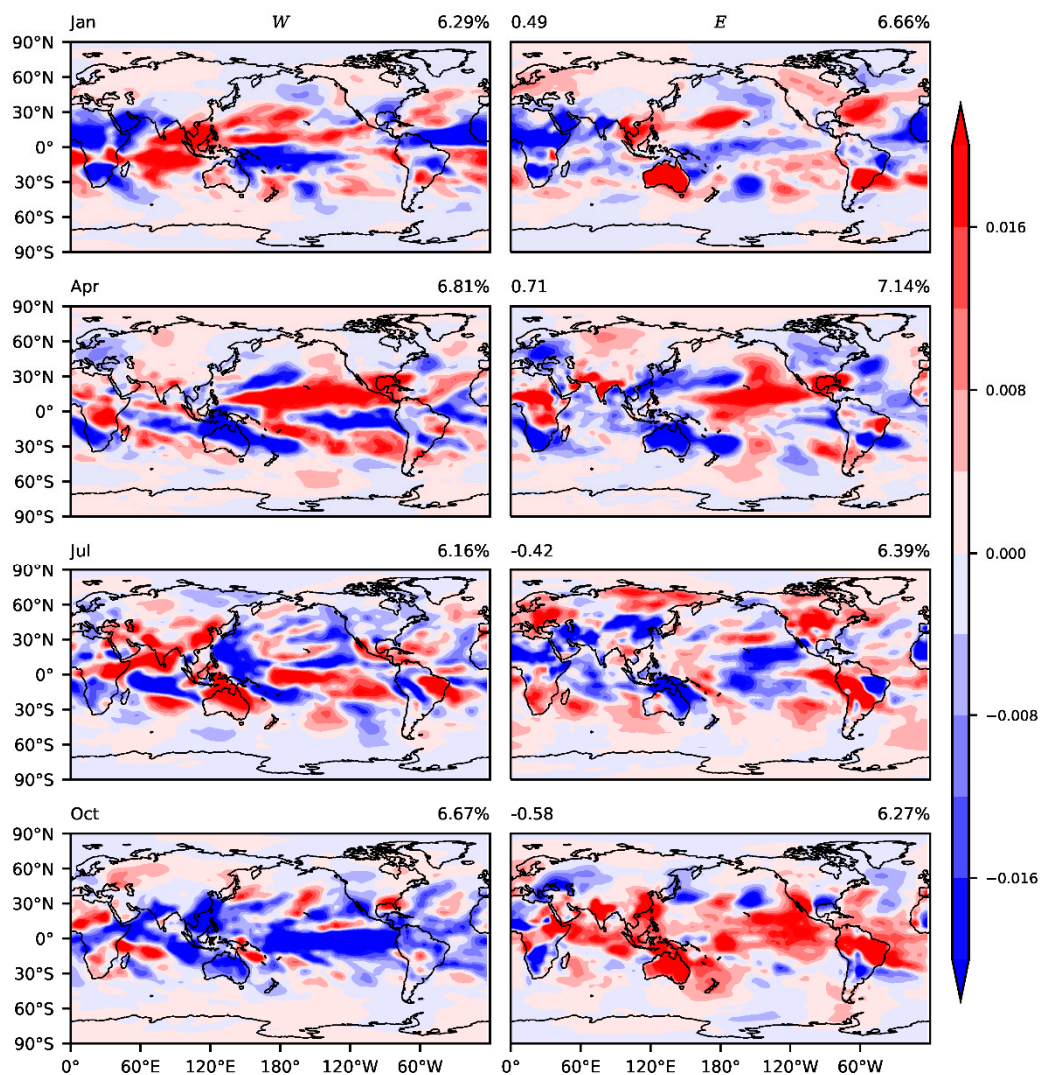
Figure S18. The third EOF modes of PW (left) and SVP (right) calculated with NCEP2. (The rows from top to bottom correspond to January, April, July, and October respectively. The percentages at the top-right of subgraphs are fractional mode variances corresponding to PW and SVP. The numbers at the upper-left corners of graphs in the right column are spatial correlation coefficients of the first modes of PW and SVP.).
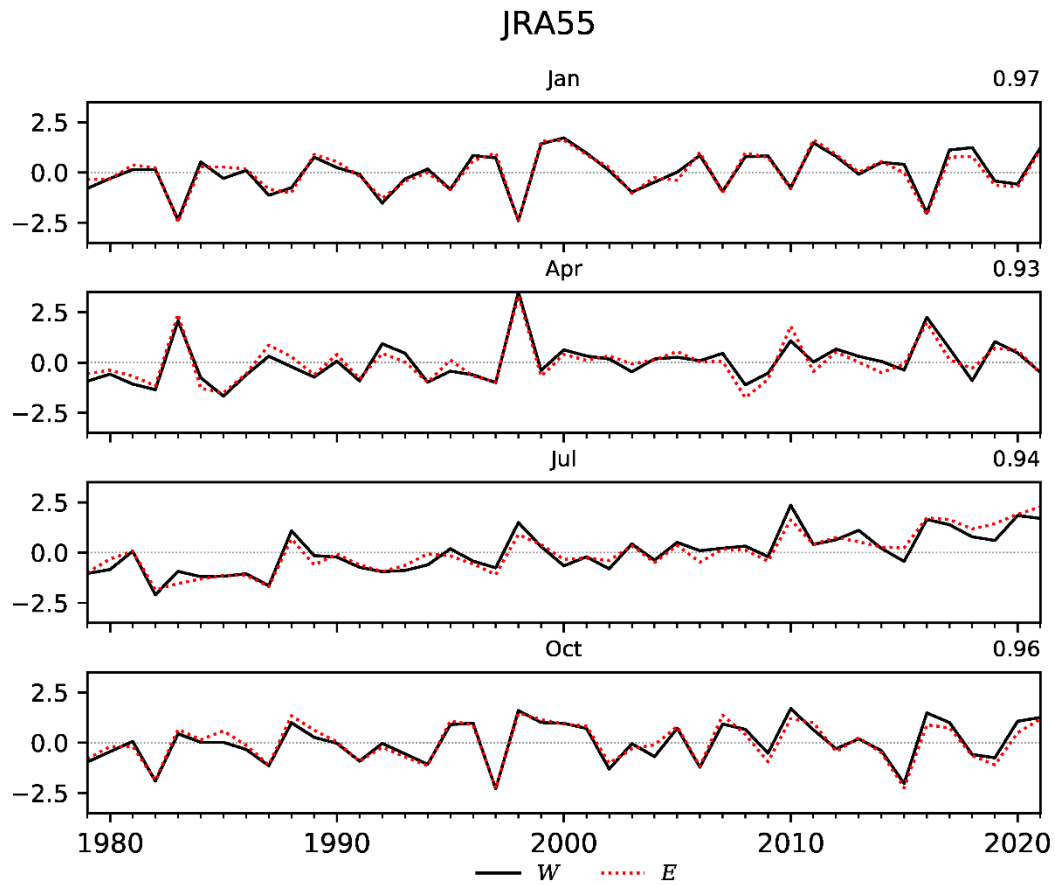
Figure S19. The principal components of EOF 1 of PW and SVP were calculated with the JRA55 dataset (scaled to unit variance). The numbers at the top-right of subgraphs are correlation coefficients of two curves.
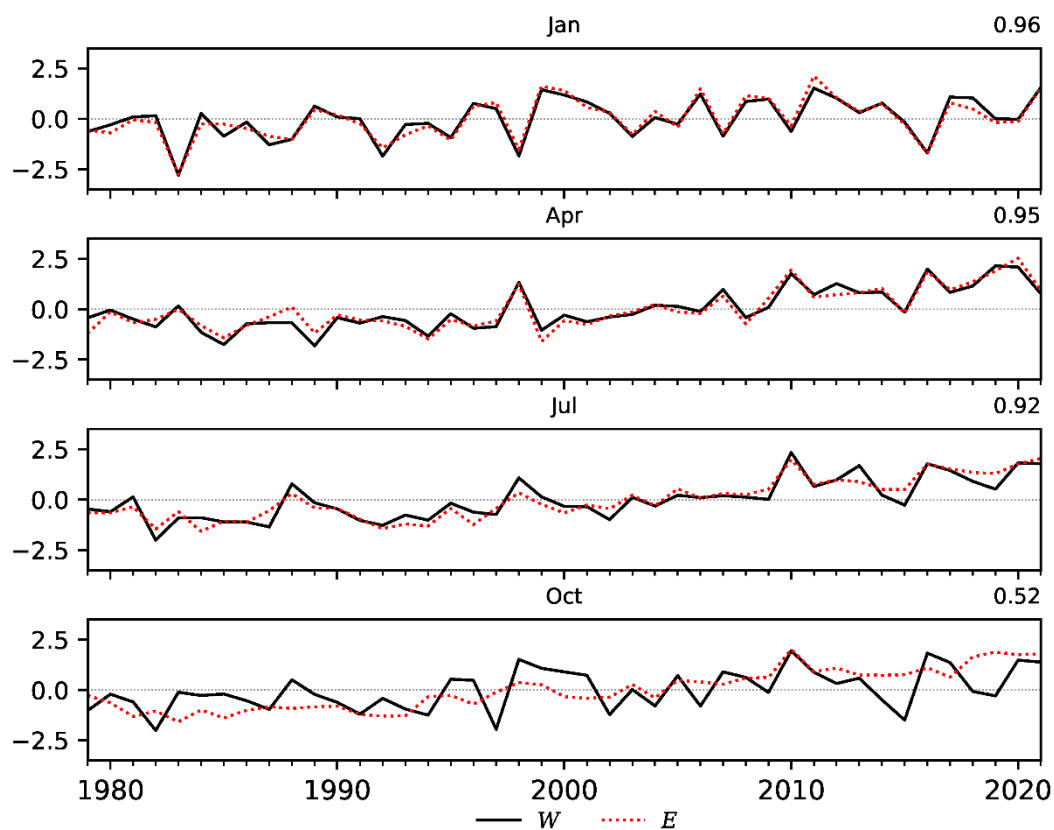
Figure S20. The principal components of EOF 1 of PW and SVP were calculated with the NCEP2 dataset (scaled to unit variance). The numbers at the top-right of subgraphs are correlation coefficients of two curves.
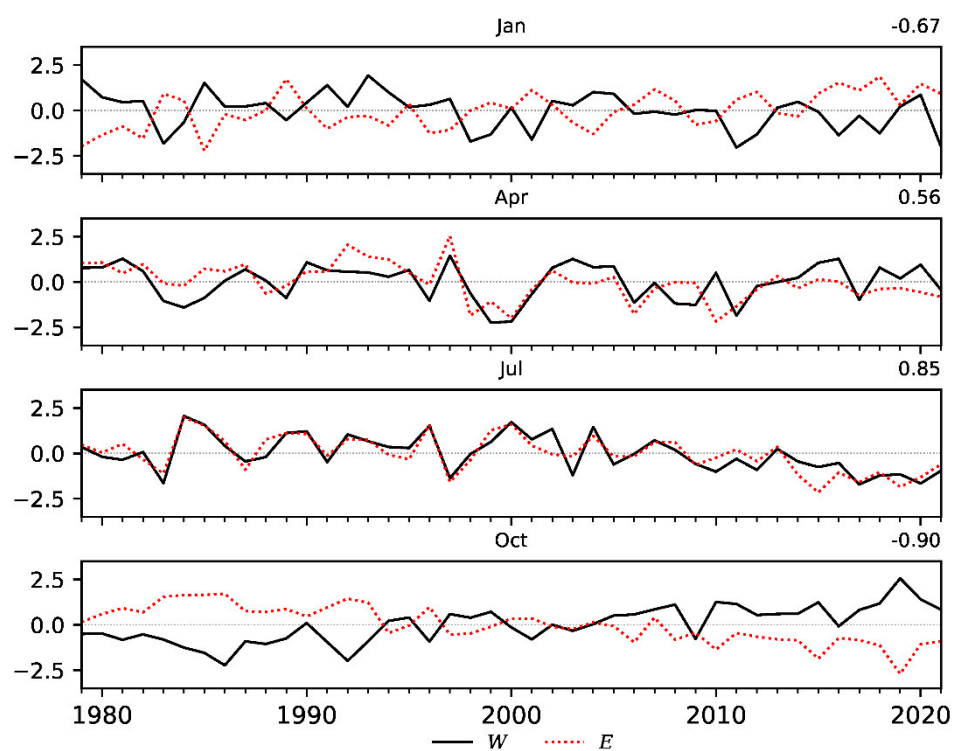
Figure S21. The principal components of EOF 2 of PW and SVP were calculated with the ERA5 dataset (scaled to unit variance). The numbers at the top-right of subgraphs are correlation coefficients of two curves.
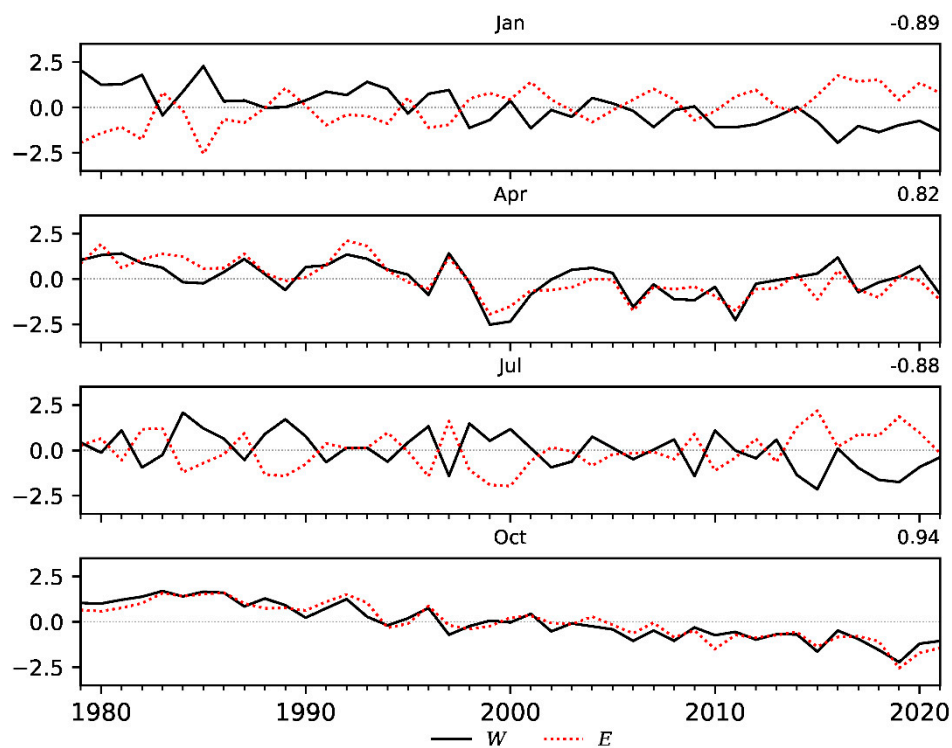
Figure S22. The principal components of EOF 2 of PW and SVP were calculated with the JRA55 dataset (scaled to unit variance). The numbers at the top-right of subgraphs are correlation coefficients of two curves.
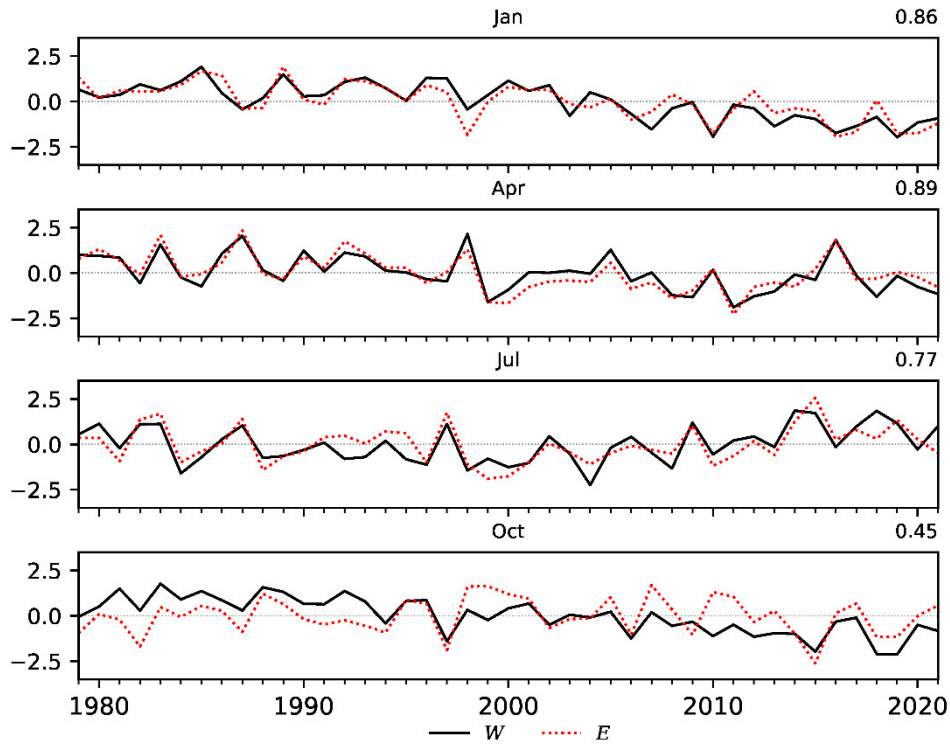
Figure S23. The principal components of EOF 2 of PW and SVP were calculated with the NCEP2 dataset (scaled to unit variance). The numbers at the top-right of subgraphs are correlation coefficients of two curves.
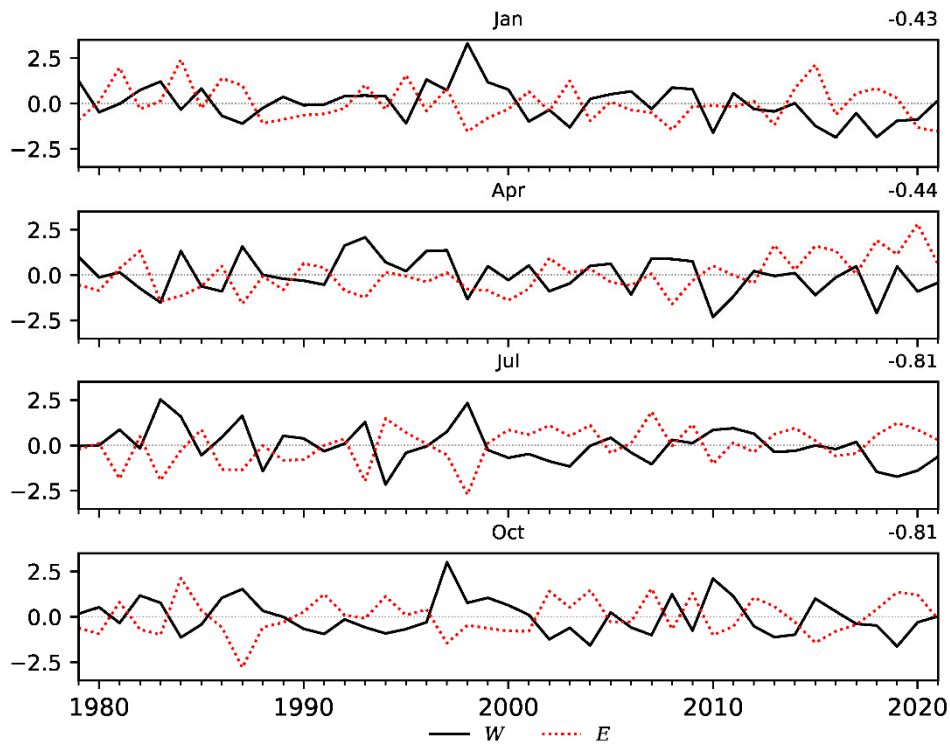
Figure S24. The principal components of EOF 3 of PW and SVP were calculated with the ERA5 dataset (scaled to unit variance). The numbers at the top-right of subgraphs are correlation coefficients of two curves.
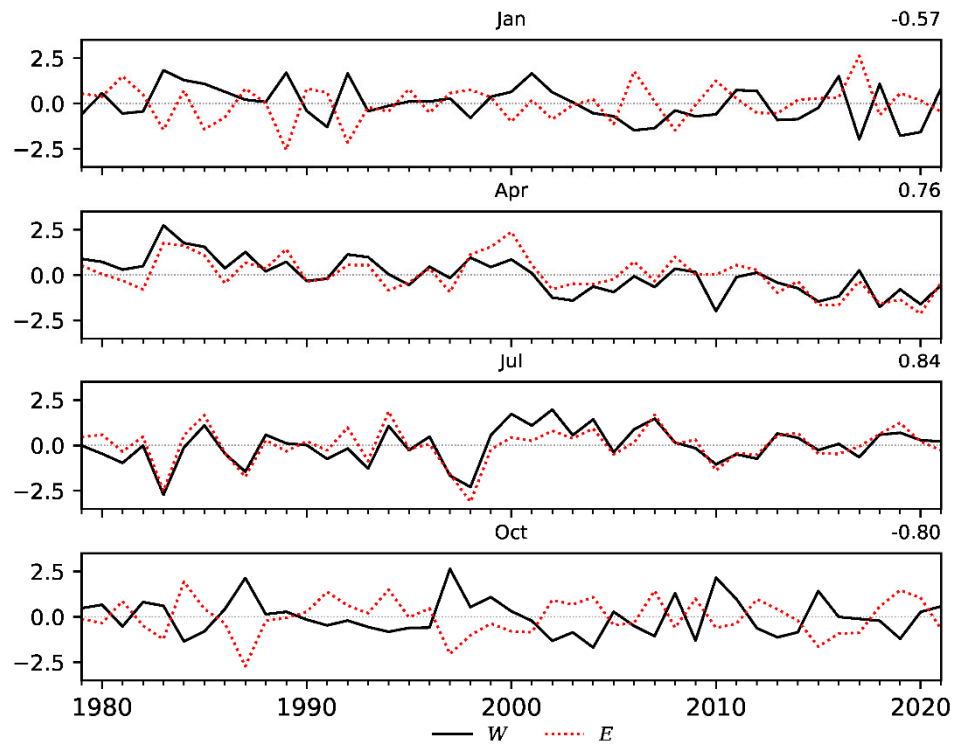

Figure S25. The principal components of EOF 3 of PW and SVP were calculated with the JRA55 dataset (scaled to unit variance). The numbers at the top-right of subgraphs are correlation coefficients of two curves.
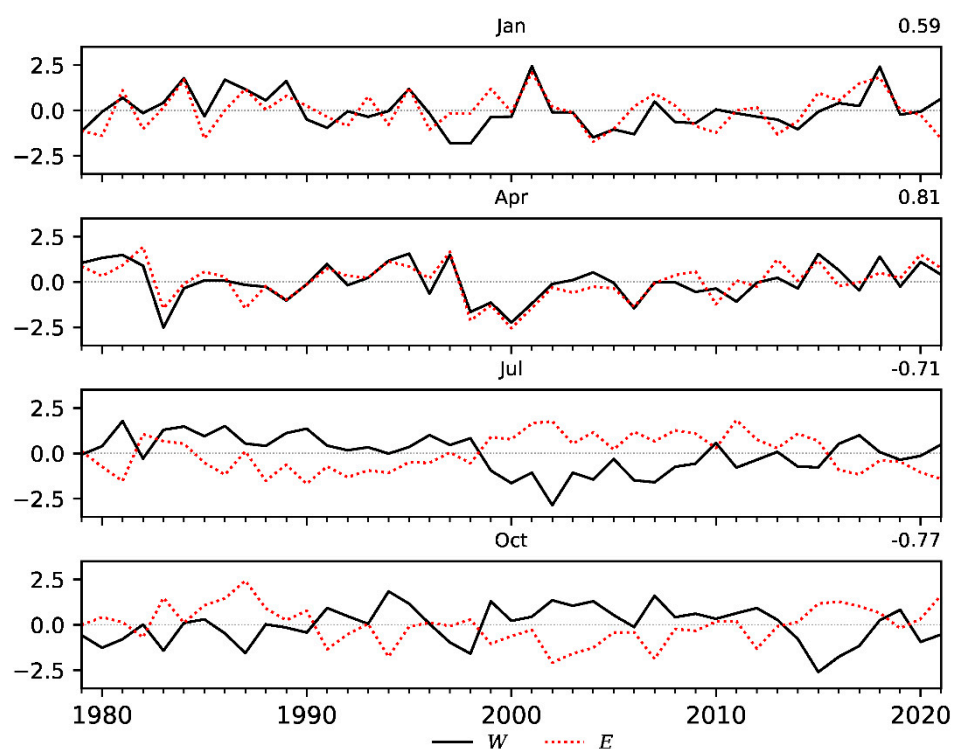
Figure S26. The principal components of EOF 3 of PW and SVP were calculated with the NCEP2 dataset (scaled to unit variance). The numbers at the top-right of subgraphs are correlation coefficients of two curves.